Portable automated radio-frequency scanner for non-destructive testing of carbon-fibre-reinforced polymer composites

B. Salski, W. Gwarek, P. Kopyt
Warsaw University of Technology, Institute of Radioelectronics, Poland

P. Theodorakeas, I. Hatziioannidis, M. Koui
National Technical University of Athens, Materials Science & Engineering Department, Greece

A.Y.B. Chong, S.M. Tan, V. Kappatos, C. Selcuk, T.H. Gan
Brunel University London, Brunel Innovation Centre, United Kingdom

ABSTRACT: A portable automated scanner for non-destructive testing (NDT) of carbon-fibre-reinforced polymer (CFRP) composites has been developed. Measurement head has been equipped with an array of newly developed radio-frequency (RF) inductive sensors mounted on a flexible arm, which allows the measurement of curved CFRP samples. The scanner is also equipped with vacuum sucks providing mechanical stability. RF sensors operate in a frequency range spanning from 10 up to 300 MHz, where the largest sensitivity to defects buried below the front CFRP surface is expected. Unlike to ultrasonic testing (UT), which will be used for reference, the proposed technique does not require additional couplants. Moreover, negligible cost and high repeatability of inductive sensors allows developing large scanning arrays, thus, substantially speeding up the measurements of large surfaces. The objective will be to present the results of an extensive measurement campaign undertaken for both planar and curved large CFRP samples, pointing out major achievements and potential challenges that still have to be addressed.

1 INTRODUCTION

Future generation of engineering structures will consist mostly of carbon composite materials, notably in the civil, aerospace, automotive and marine industries due to their performance and structural efficiency. The modes of failure in composite intensive structures such as the increasingly popular carbon-fibre-reinforced polymer (CFRP) composite reinforced concrete beams [1-3] or the recent operational aircraft, Boeing 787 Dreamliner (with 50% composite) [4], are not fully known as they are still near the beginning of their design life. However, it is clear that these CFRP materials are susceptible to internal impact damage, not visible with an un-aided eye at the surface. In spite of this, inspections at the point of manufacture and in service is largely manual with consequent low area coverage. Operation downtime is usually inevitable during scheduled or unscheduled inspection. Common non-destructive testing (NDT) techniques utilized for CFRP include ultrasonic testing (UT) [5-6], eddy current testing (ECT) [7-8], shearography [9], microwave and millimeter wave [10-11]. However, results obtained are difficult to interpret for most NDT techniques due to the intrinsic anisotropy of the structure. Moreover, there are requirements for specific techniques which may be easily applicable in-situ. As a result of the recent successful development of the planar coupled spiral inductors tailored for the NDT of CFRP composites [12-13], the sensor and auxiliary modules were subject to further development in which a line array of sensors is realized. The sensor array is integrated with a portable automated scanner. The fundamental principle of operation is based on radio-frequency (RF) inductive approach where the coupling between the two inductors tangential to the surface of the material under test (MUT) is measured. For brevity, this technique is referred as RF inductive testing (RFIT) in this paper. Experiments were carried out to validate the system prototype on both planar and curved CFRP composites with typical buried and surface defects. The results clearly demonstrate the applicability of such automated RFIT system for reliable and efficient CFRP inspection.

2 SCANNER

The whole NDT system, as shown in Fig. 1, consists of the scanner with a sensor arm, data acquisition board (DAQ), and a PC station.

2.1 *Chassis*

One of major objectives was to minimize a scanner's weight, while providing high scanning rates, good resolution, positioning repeatability in both absolute and relative coordination systems, involving

the minimum degrees of freedom. For that reason, an important functional requirement was the development of an ergonomic portable chassis with the weight less than 10kg. Furthermore, it should provide the necessary space for seamless integration of all modalities that will implement the requested functional requirements of the scanner. Based on the aforesaid, the scanner frame was designed and manufactured through the use of two aluminum plates as presented on a schematic design in Fig. 2. The chassis was secured via the application of four tubes with collars that interconnect the two layers of aluminum plates. The aluminum plates were pre-cut with all necessary cut-outs and bores so as to be able to attach all necessary parts, gantry, motor supports, electronics, and pneumatic systems. The chassis structure has the advantage that all parts are accessible and can be removed readily for repair or replacement. It can be easily disassembled, machined if modifications are necessary during service period and reproduced on request. The overall size of the chassis frame is 600x400x250 mm^3.

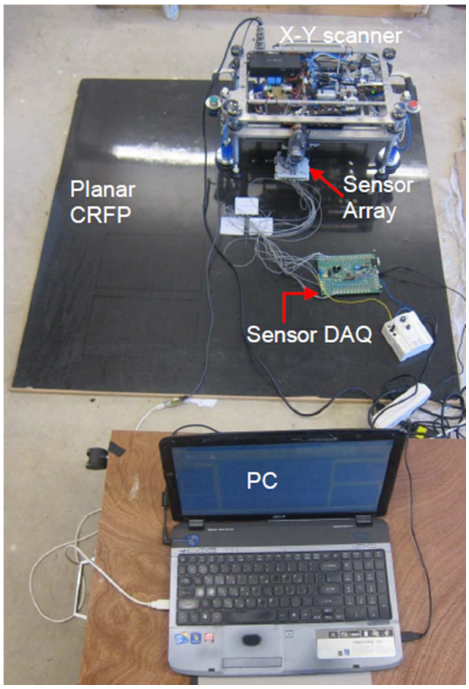

Figure 1. NDT scanner setup.

The main function of the x-y gantry system is to implement a scanning motion of a sensor arm. For that purpose, an Igus Drylin stage drive product was selected. It provides lubricant-free linear axles that are driven either by trapezoidal thread, steep thread or toothed belt. The user can choose a suitable individual solution from lightweight solid plastic units up to massive stainless steel solutions. For our application trapezoidal threads with 2 mm pitch were chosen for both X and Y directions. Along with robust design of these components, their main features include ruggedness and insensitivity to dirt, water, chemicals, heat or impacts.

Magnetic encoders have a resolution of 1024 ticks per shaft revolution. One revolution is converted to a linear motion of 2 mm with a resolution of 10μm per revolution of the DC motors. The power source is mounted within the chassis boundaries and provides the scanner with voltage supply options of 5-12-24V DC. The scanner is controlled via RS-485 protocol converted to USB before it is connected to the PC.

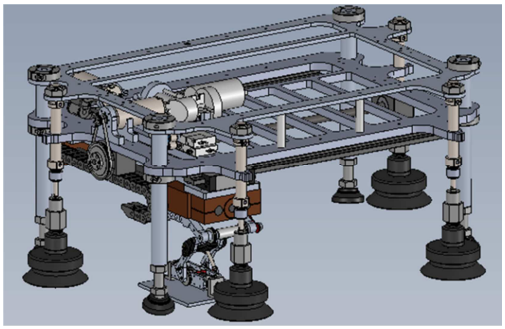
Figure 2. Scanner platform with XY precision translators, sensor arm and vacuum sucks.

Another function of the scanner is the attachment to the composite's surface. Due to operational principles of the inspection method and the composite material characteristics, it was not possible to implement magnets and clamping systems for the robust mounting of the scanner. For that reason, plastic suction cups were developed which satisfy three crucial preconditions: a) there is no magnetic field interference with RF sensors, and b) they cause absolutely no surface damage to the MUT. The mounting of the scanner is performed by the following procedure. Initially, the operator places the scanner on the MUT's surface, ensuring that the supporting legs and the plastic cups are conformed on the surface. Subsequently, pressure can be produced to the cups by pressing an air compressor activation button. As a result of a network pressure of 8 bar, the scanner becomes firmly attached to the surface.

2.2 *Sensor arm*

Sensor arm, as shown in Fig. 3, is a mounting platform for the array of RF sensors. It is made of aluminum housed with bearings, pivot brackets, and springs to produce a lab jack mechanism with better conformance of the sensors to the MUT's surface. RF sensors are placed in PA6 plastic protection pads, which are mounted to a holder arm with the aid of a plastic holder plate to prevent any large metallic parts in the vicinity of the sensors. Although mounting pads indicated in Fig. 4 fit precisely to the plastic protection pads, the attachment can be further enhanced with thermoplastic adhesive. The dimensions of the holder plate are 100x120 mm^2 with a thickness of 8 mm.

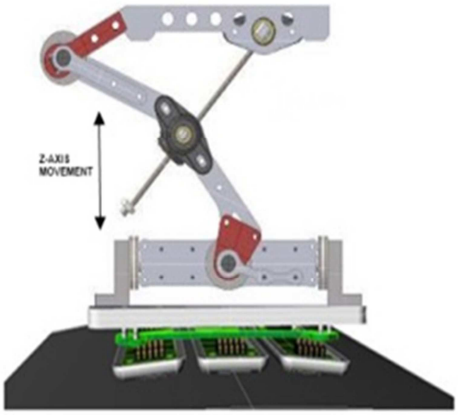

Figure 3. Sensor flexible arm.

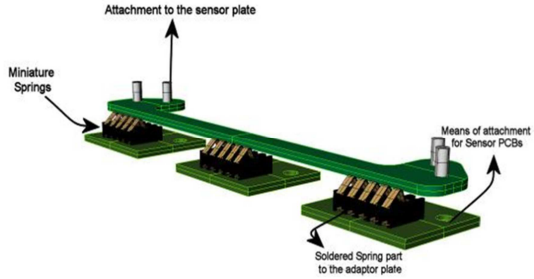

Figure 4. Mounting pad of RF sensors.

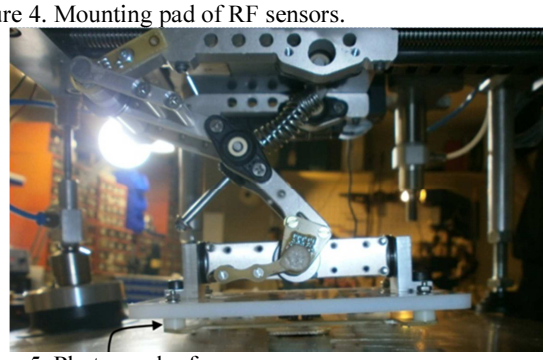

Figure 5. Photograph of a sensor arm.

Vertical force pushing the sensors to the CFRP surface is provided by the lab jack mechanism that drives a passive spring on the outside of a telescopic pair shown in Fig. 4. An exerted force over the sensor plate is adjusted by the use of springs in order to maintain a firm contact with the MUT's surface during a sliding movement of the sensors. The total travel distance on the z-axis is 40 mm, enabling the application of proper pressure to the sensor plate, in order to ensure its smooth conformance on curved surfaces. The vertical displacement can be monitored with an integrated absolute encoder.

2.3 *RF sensors*

Sensor array is made in the form of a line of RF inductors manufactured on a printed circuit board as shown in Fig. 6. Single measurement utilizes two adjacent inductors treated as primary and secondary windings of a transformer. As a result, there are N-1 measurement points for N aligned inductors.

If RF sensors are attached to the MUT's surface with the aid of the sensor arm, a magnetic field penetrates the MUT provided that the penetration depth d_p is large enough at a given frequency. For instance, conductivity of CFRP composites is usually in the range of $\sigma = 10^4$ S/m, which means d_p is over 1 mm for frequencies below ca. 30 MHz. It implicitly determines the frequency range for RF inductors if the thickness of CFRP panels is given.

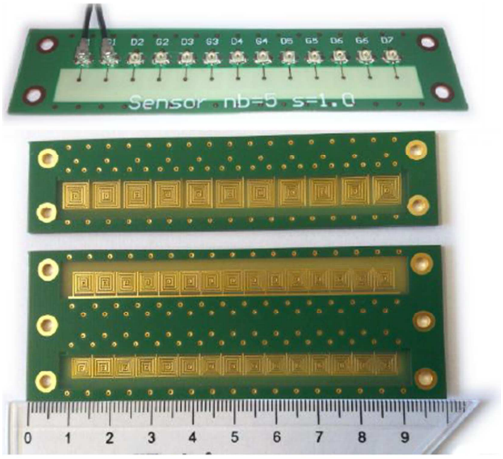

Figure 6. Exemplary RF sensors.

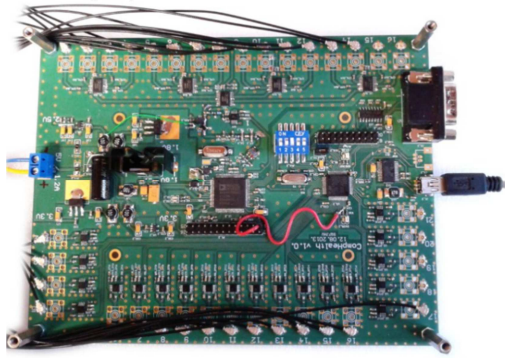

Figure 7. Data acquisition board.

2.4 *Data acquisition board*

In the view of the above considerations of the frequency range of operation of the RF sensors, electronic circuitry, dedicated to the measurement of the number of individual sensor channels, has been developed (see Fig. 7). The main role in that system is played by a direct digital synthesizer (DDS), controlled with a 32-bit microcontroller, which also serves as an interface with a PC host station. DDS generates signals spanning from 20 MHz up to 300 MHz, as this is the spectrum where the largest sensitivity to defects buried in ca. 1mm thick CFRP panels is expected. The signal is multiplexed to all measurement channels in a sequential form. Each channel is also equipped with its individual logarithmic wideband power detector. As a result, each measurement shot provides the whole spectrum of power transmission through each coupled sensor pair, as indicated in Fig. 6.

3 MEASUREMENTS

Characterization of flat and curved CFRP panels will be presented in this Section. Both panels, manufactured by ATARD [14], consist of four layers of CFRP twill immersed in epoxy resin. All the samples have been measured with a single line of RF inductive sensors shown at the top of Fig. 6 mounted in the scanner depicted in Fig. 1 with 12 measurement pairs. As the scanning step has been set to 2 mm, an image of a 300x200 mm^2 surface consists of over 15 000 steps, which means that the scanner has to undertake 1250 incremental shifts across the surface. That number can be further decreased if additional sensor lines are exploited in the scanner (see Fig. 3), which will be the subject for future enhancements of the system.

3.1 *Flat CFRP panel*

The flat CFRP panel is shown in Fig. 8. As it can be noticed, a few types of defects have been intentionally introduced, such as holes, bubbles, cracks, and delamination. Figure 9 shows RF images stored at two distinct frequencies. The image at 50 MHz clearly indicates a large hole, which is not visible at the front surface of the panel. It can be partially confirmed by the lack of the hole at the RF image at 200 MHz, which due to a substantially decrease penetration depth is sensitive mostly to the CFRP features, which are shallowly buried under the top surface of the panel. In particular, regular fracture appearing in Fig. 9b is correlated with the orientation of the front CFRP twill.

Figure 8. Flat CFRP panel.

Figure 10 indicates an RF image measured at 20 MHz at the areas of the flat CFRP panel shown in Fig. 8, where buried bubbles are introduced by the manufacturer. Indeed, several tiny fluctuations can be observed in the central part and the right side of the image, while the changes at the left side of the image are rather smooth and results mostly due to slight misalignments of the CFRP twill.

Subsequently, Fig. 11 shows vertical cracks buried at selected regions of the CFRP sample. As the cracks are visible even at 300 MHz, it can be concluded that the defects are spanning almost across the total thickness of the sample, although those are not visible with a naked eye.

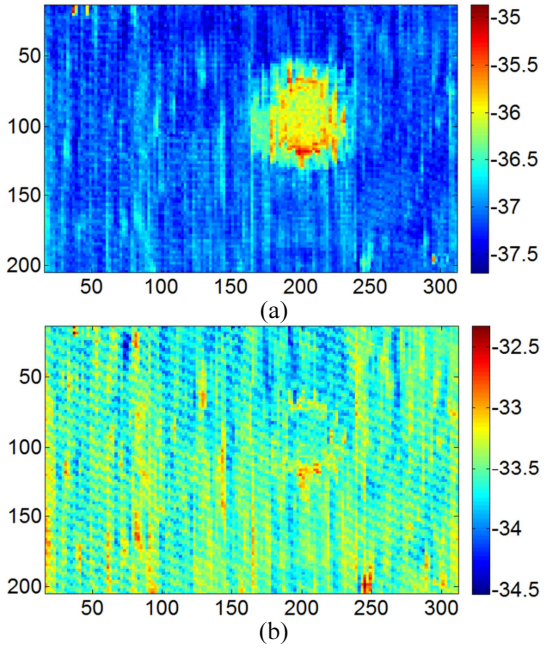

Figure 9. Hole buried in the CFRP sample shown in Fig. 8a measured at (a) 50 MHz and (b) 200 MHz.

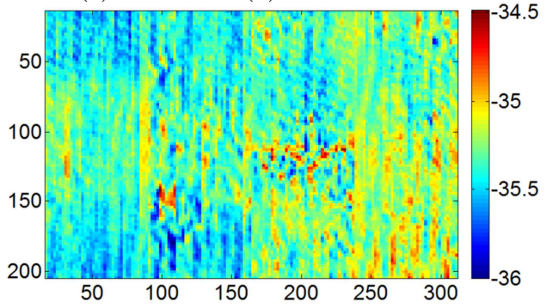

Figure 10. Specific bubbles buried in the CFRP sample shown in Fig. 8a measured at 20 MHz.

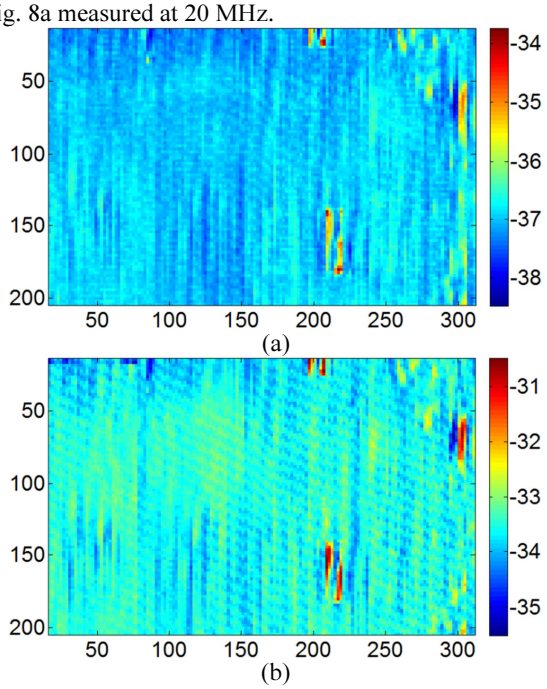

Figure 11. Cracks buried in the CFRP sample shown in Fig. 8a measured at (a) 20 MHz and (b) 300 MHz.

Eventually, Fig. 12 shows delamination buried in the CFRP sample shown in Fig. 8a measured at two distinct frequencies. As it can be noticed in Fig. 12a, there is a large deep minimum at a left side of the image, where the defect is expected and which cannot be noticed at 300 MHz indicating its deeper location.

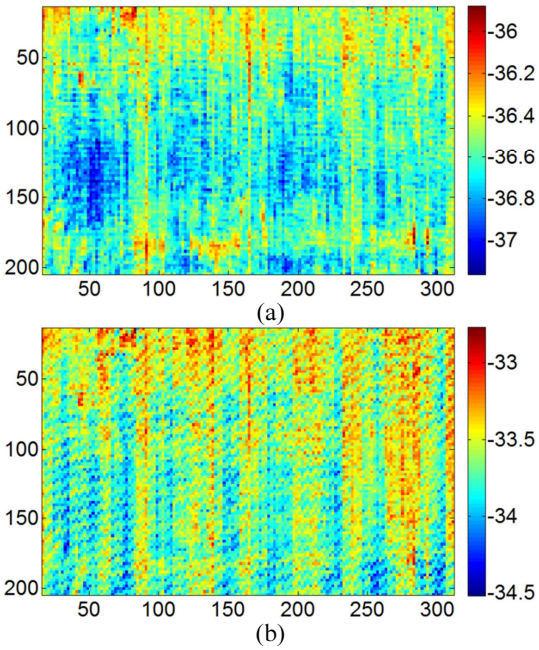

Figure 12. Delamination buried in the CFRP sample shown in Fig. 8a measured at (a) 20 MHz and (b) 300 MHz.

3.2 *Curved CFRP panel*

Figure 12 shows the sample of a curved CFRP panel with several types of defects introduced in a similar way as in the flat sample. Curvature radius of the panels is ca. 1.5 m. As it will be shown, measurement of curved panels brings additional issues related to uneven attachment of the sensor line to the surface, which has to be de-embedded from raw measurement data.

Figure 13 depicts specific bubbles occurring at a front surface of the curved CFRP panel. The corresponding RF image consists of four individual stripes due to the chosen direction of the sensor indicated in Fig. 13. Figure 14 shows the obtained RF image, where those four stripes are well visible due to the aforementioned uneven attachment of the sensor line to the curved surface. Fortunately, it results in a linear trend occurring in power transmission measured across the sensor line, so it can be estimated and removed at a post-processing stage. Consequently, Fig. 14b is smoother enabling better recognition of the bubbles, the location of which corresponds very well with those shown in Fig. 13.

Figures 15-17 show another types of defects measured with the RF scanner at 20 MHz. In the case of delamination, it can be seen in the middle of the image in Fig. 15. In addition to that, there is also some vertical defect visible at the left side of the RF image shown in Fig. 15, which may be some buried crack unintentionally introduced by the manufacturer.

Subsequently, Fig. 16 indicates several cracks measured on the curved CFRP sample, while a hole can be clearly observed in the top right corner of the image in Fig. 17. Similarly to the unintentional crack depicted in Fig. 15, there is a horizontal fault visible in Fig. 17, which has not been explicitly highlighted by the manufacturer.

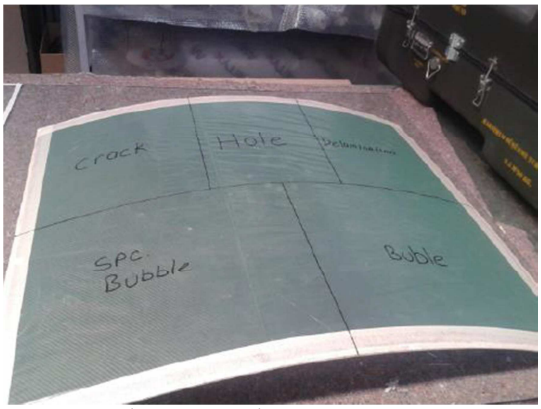

Figure 12. Curved CFRP panel.

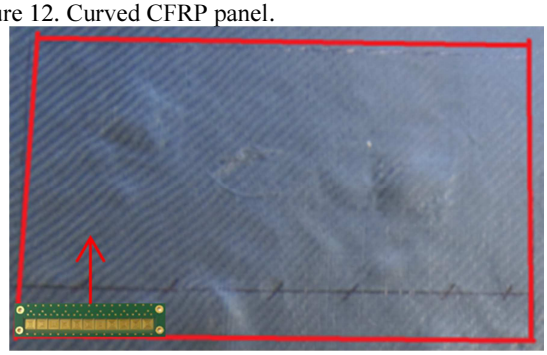

Figure 13. Specific bubbles on the curved CFRP sample shown in Fig. 12.

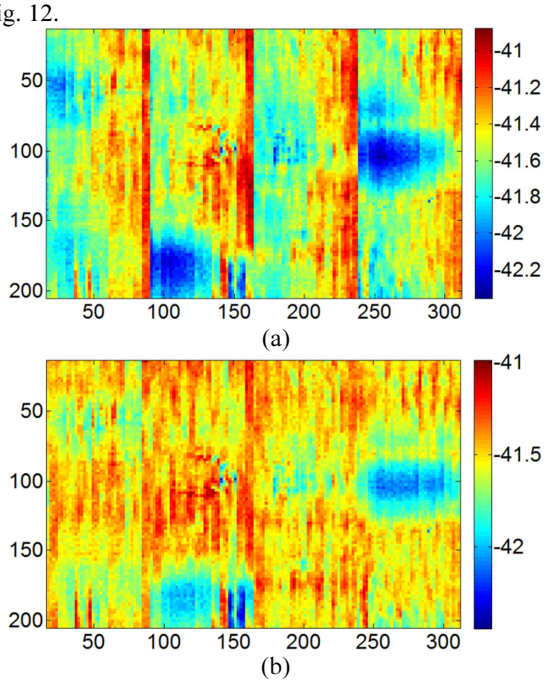

Figure 14. Specific bubbles on the CFRP sample shown in Fig. 13 and measured at 20 MHz. (a) Raw data. (b) Linear trend removed.

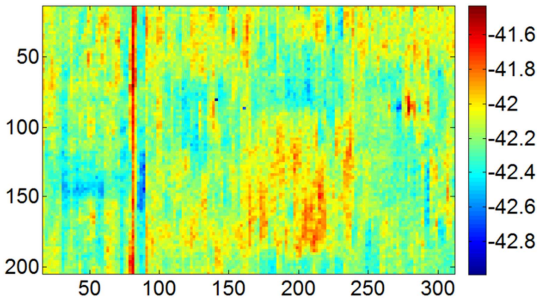

Figure 15. Delamination buried in the CFRP sample shown in Fig. 13 measured at 20 MHz. Linear trend is removed.

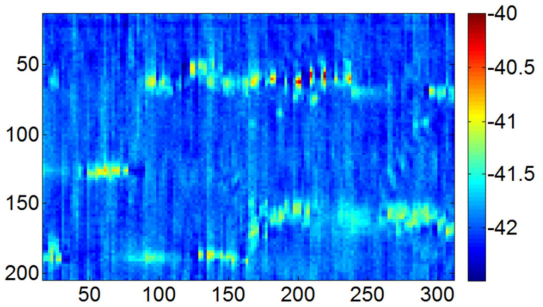

Figure 16. Cracks buried in the CFRP sample shown in Fig. 13 measured at 20 MHz. Linear trend is removed.

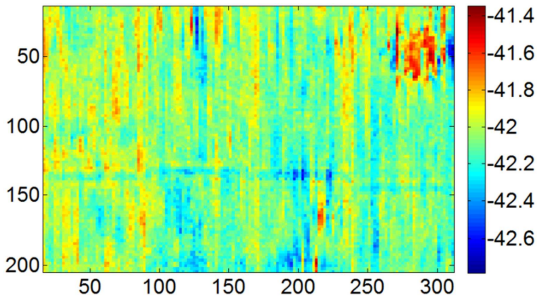

Figure 17. Holes buried in the CFRP sample shown in Fig. 13 measured at 20 MHz. Linear trend is removed.

4 ACKOWLEDGEMENT

The research leading to these results has received funding from EU 7th Framework Programme managed by REA under grant agreement no. 314935. Part of this work was also funded by the Polish National Ministry of Science and Higher Education under grant agreement no. 2826/7.PR/2013/2.

The research has been undertaken as a part of the project entitled "Radio Frequency Sensing for Non-Destructive Testing of Carbon Fibre Reinforced Composite Materials for Structural Health Monitoring" – Comp-Health, in the collaboration between the following organizations: E.T.S. Sistemi Industriali srl, Kingston Computer Consultancy Limited, Nemetschek ood, Atard a.s., UAB Elmika, Warsaw University of Technology, National Technical University of Athens and Brunel Innovation Centre of Brunel University London.

5 REFERENCES

[1] Y. Zhou, M. Guo, F. Zhang, S. Zhang, and D. Wang, "Reinforced concrete beams strengthened with carbon fibre reinforced polymer by friction hybrid bond technique: Experimental investigation," *Material and Design*, vol. 50, pp. 130–139, 2013.

[2] R. Garcia, Y. Helal, and K. Pilakoutas, "Bond behavior of substandard splices in RC beam externally confined with CFRP," *Construction and Building Materials*, vol. 50, pp. 340–351, 2014.

[3] X.L. Zhao and L. Zhang, "State-of-the-art review on FRP strengthened steel structures," *Engineering Structures*, vol. 26, no. 8, pp 1808-1823,2007.

[4] Available: www.compositesworld.com/articles/boeing-787-update, last accessed on 26/03/2015.

[5] C. Scarponi and G. Briotti, "Ultrasonic technique for the evaluation of delaminations on CFRP, GFRP, KFRP composite materials," *Composites Part B: Engineering*, vol. 31, no. 3, pp. 237–243, 2000.

[6] M.D. Farinas, T.E.G. Alvarez-Arenas, E.C. Aguado, and M.G. Merino, "Non-Contact Ultrasonic Inspection of CFRP Prepregs for Aeronautical Applications during Lay-Up Fabrication," IEEE IUS Book Series, pp. 1586–1589, 2013.

[7] J. Chen, H.L. Ji, J.H. Qiu, T. Takagi, T. Uchimoto, and N. Hu, "Novel electromagnetic modeling approach of carbon fibre-reinforced polymer laminate for calculation of eddy currents and eddy current testing signals," *Journal of Composite Materials*, vol. 49, no. 5, pp. 617-631, 2015.

[8] G. Mook, R. Lange, and O. Koeser, "Non-destructive characterization of carbon-fibre-reinforced plastics by means of eddy-currents," *Composites Science and Technology*, vol. 61, no. 6, pp. 865–873, 2001.

[9] F. Taillade, M. Quiertant, and K. Benzarti, "Shearography and pulsed stimulated infrared thermography applied to a nondestructive evaluation of FRP strengthening systems bonded on concrete structures," *Construction and Building Materials*, vol. 25, pp. 568574, 2011.

[10] M. Ravuri, M. Abou-Khousa, S. Kharkovsky, R. Zoughi and R. Austin, "Microwave and Millimeter Wave Near-Field Methods for Evaluation of Radome Composites," *Review of Progress in Quantitative Nondestructive Evaluation Quantitative Nondestructive Evaluation*, vol. 27B, pp. 976-981, 2008.

[11] S. Kharkovsky and R. Zoughi, "Microwave and Millimeter Wave Nondestructive Testing and Evaluation – Overview and Recent Advances," *IEEE Instrumentation and Measurement Magazine*, vol. 10, no. 2, pp. 26-38, 2007.

[12] B. Salski, W. Gwarek, and P. Korpas, "Electromagnetic inspection of carbon-fiber-reinforced polymer composites with coupled spiral inductors," *IEEE Trans. Microw. Theory Techn.*, vol. 63, no. 7, pp. 1535–1544, 2014.

[13] B. Salski, W. Gwarek, P. Korpas, S. Reszewicz, A.Y.B. Chong, P. Theodorakeas, I. Hatziioannidis, V. Kappatos, C. Selcuk, T.H. Gan, M. Koui, M. Iwanowski, and B. Zielinski, "Non-destructive testing of carbon-fibre-reinforced polymer materials with a radio-frequency inductive sensor," *Compos. Struct.*, vol. 122, no. 104, Nov. 2014.

[14] ATARD, Defence and Aerospace Industry Advanced Technology Applications Research and Development Inc., private communication, February 2013.